Transonic Airfoil Analysis and Design Using Cartesian Coordinates

Leland A. Carlson*
Texas A&M University, College Station, Tex.

An inverse numerical technique for designing transonic airfoils having a prescribed pressure distribution is presented. The method uses the full potential equation, inverse boundary conditions, and Cartesian coordinates. It includes simultaneous airfoil update and utilizes a direct-inverse approach that permits a logical method for controlling trailing edge closure. The method also can be used for the analysis of flowfields about specified airfoils. Comparison with previous results shows that accurate results can be obtained with a Cartesian grid. Examples show the application of the method to design aft-cambered and other airfoils specifically for transonic flight.

Introduction

A NUMERICAL method for the design of transonic airfoils should not only be accurate but also be as simple as possible in concept and approach. It should use coordinate systems, input variables, and boundary condition treatments that can be understood easily by the user. In addition, it would be desirable if the method yielded the airfoil design shape for a given set of conditions with little or no iteration, and used or computed nose and tail shapes that are aerodynamically and structurally reasonable. Finally, it should be able to handle both shocked and shockless flows and be suitable not only for complete design, but also airfoil modification.

Previous design methods and programs either have worked with the hodograph equations,[1,2] used direct optimization techniques[3], or tried the inverse approach.[4-7] Of these, probably the best known are the hodograph methods of Nieuwland[1] and of Bauer, Garabedian, and Korn.[2] Although these methods yield excellent accurate results, they are restricted to shock-free solutions, which may have adverse drag, pitching moment, and boundary-layer separation characteristics at off-design conditions.[8] Further, they are difficult from the user standpoint in that they involve complex mappings and transformations and require complicated initial input conditions. As a consequence, the hodograph methods sometimes require a large number of trial solutions before an acceptable airfoil design is achieved,[7] and they are not suitable for simple airfoil modification, since there is no way of changing only part of the solution.

Another design technique is to use a direct method (airfoil prescribed) to analyze the flow about a given airfoil, and then, based upon this result, to modify the airfoil in an attempt to satisfy the design conditions. Usually this approach requires extensive experience on the part of the user and a large number of iterations. It can, however, yield good results. For example, Hicks, Murmann, and Vanderplaats[3] recently have developed a very promising direct design procedure by combining a small perturbation analysis program with an optimization program based on the method of feasible directions.

The last design formulation is the inverse method in which the airfoil surface pressures or velocities are specified, and the airfoil shape is subsequently determined. Admittedly this approach requires knowledge of what would be a desirable pressure distribution, but this characteristic probably is understood by the designer as well as, if not better, than any other. Furthermore, the designer can a priori select a pressure distribution that will yield a given lift and moment, have a reasonable supersonic zone, behave desirably with respect to boundary-layer separation, and satisfy other transonic flow criteria. Of course, the resultant airfoil design shape may or may not be physically and structurally reasonable.

The inverse approach was initially pursued by Erdos, Baronti, and Elzweig,[4] by Steger and Klineberg,[5] and later by Carlson.[6] All used the small perturbation equations and formulated the problem in a direct-inverse manner. That is, the leading edge shape was specified and that region was solved directly, whereas on the remainder of the airfoil the pressure was prescribed and the shape was computed. These results established that inverse results consistent with direct calcualtions could be obtained by use of the perturbation potential. However, it was determined that the inverse approach, using the small perturbation equations, tended to become inaccurate for thick and blunt-nosed airfoils.

In order to overcome this problem, Tranen[7] applied the complete equations to the inverse problem by modifying the conformal mapping relaxation solution technique of Garabedian and Korn to use the pressure distribution boundary condition. Since this technique maps the computational grid to match the airfoil surface, Tranen was forced to apply the boundary conditions at the surface of some assumed airfoil. Only after the relaxation process had converged could a new shape be computed; usually, because of the difference between where the boundary conditions actually were and where they should have been applied, the resultant shape was not completely compatible with the input pressure distribution. Tranen solved this problem by resorting to, for each case, a series of inverse-direct-inverse-direct, etc., calculations in which the pressure distribution was modified prior to each inverse calculation. This was done in an attempt to achieve convergence, which was defined as when the C_p distribution from a direct computation agreed with that used as input in the previous inverse run.

The purpose of this paper is to present a new numerical method suitable for the analysis, design, or modification of subsonic and transonic airfoils. In order to achieve accuracy, the method utilizes the full inviscid potential flow equation; and in order to remain simple, it solves the problem in a stretched Cartesian grid system. The resultant working computer program has several unique features. First, it can be used in either the direct (analysis) mode in which the airfoil shape is prescribed and the flowfield and surface pressures are determined, or in the direct-inverse (design) mode in which an initial nose shape is given along with the pressure distribution

Presented at the AIAA 2nd Computational Fluid Dynamics Conference, Hartford, Conn., June 19-20, 1975; submitted June 20, 1975. This research was primarily supported by NASA Grant NGR-44-001-157 and NSG 1174, and partially by the NASA-ASEE Summer Faculty Fellowship Program and the Texas Engineering Experiment Station.

Index category: Subsonic and Transonic Flow.

*Associate Professor, Department of Aerospace Engineering. Member AIAA.

on the remainder of the airfoil, and the flowfield and acutal airfoil shape are computed. Second, unlike previous methods, the present program determines the airfoil shape simultaneously with the flowfield relaxation solution. Thus, when the converged solution is achieved, an airfoil design compatible with the input pressure distribution is known, and iteration is not required.

Problem Formulation

The exact equation for the perturbation potential function for two-dimensional compressible flow can be written in Cartesian coordinates as

$$(a^2-U^2)\phi_{xx}-2UV\phi_{xy}+(a-V^2)\phi_{yy}=0 \tag{1}$$

where the subscripts denote partial differentiation, and the velocity components are given by

$$U=q_\infty(\cos\alpha+\phi_x)$$

$$V=q_\infty(\sin\alpha+\phi_y) \tag{2}$$

The appropriate boundary condition at infinity is[9]

$$\phi=(-\Gamma/2\pi)\tan^{-1}[\beta\tan(\theta-\alpha)] \tag{3}$$

where θ is the polar angle and Γ is the circulation.

In order to be able to apply this boundary condition directly, the coordinate stretching represented in Fig. 1 was selected. Here the x-y plane is the physical plane, $\xi-\eta$ represents the computational plane, and each is subdivided into three regions. The stretching is symmetrical about the origin and is given by

$$x=x_4+A_2\tan[(\pi/2)(\xi-\xi_4)]$$

$$+A_3\tan[(\pi/2)(\xi-\xi_4)^3] \tag{4}$$

in region III, and by

$$x=\xi(a+b\,\xi^2) \tag{5}$$

in region II. The constants a and b are determined by the requirements $x=x_4$ and $dx/d\xi=\pi A_2/2$ at $\xi=\xi_4$. The constant A_2 controls the grid spacing in the vicinity of x_4, usually near the leading the trailing edges; whereas A_3 determines the physical location of the grid line adjacent to the grid edge.

In the y-direction, the stretching relationship is given by

$$y=A_1\tan[(\pi/2)\eta] \tag{6}$$

where A_1 controls the grid size near the airfoil. Notice that the stretchings map the infinite physical x,y plane into the finite computational plane

$$-(1+\xi_4)\le\xi\le 1+\xi_4 \qquad -1\le\eta\le 1 \tag{7}$$

where ξ_4 determines the amount of the computational plane confined to the vicinity of the airfoil. As a result, the governing equations written in terms of the independent computational variables ξ and η are

$$(a^2-U^2)f(f\phi_\xi)_\xi-2UVfg\phi_{\xi\eta}$$

$$+(a^2-V^2)g(g\phi_\eta)_\eta=0 \tag{8}$$

$$U=q_\infty(\cos\alpha+f\phi_\xi)$$

$$V=q_\infty(\sin\alpha+g\phi_\eta) \tag{9}$$

where $f=d\xi/dx$ and $g=d\eta/dy$.

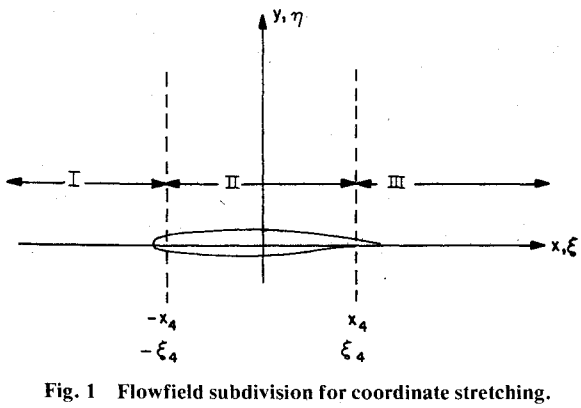

Fig. 1 Flowfield subdivision for coordinate stretching.

Finite-Difference Scheme

In order to avoid, at supersonic points, difficulties associated with nonalignment of the coordinates and the flowfield, a rotated finite-difference scheme is used. In this approach[10,11] the principal part of the governing differential equation can be written in coordinates parallel and perpendicular to the local velocity vectors, S and N, respectively, as

$$(1-q^2/a^2)\phi_{SS}+\phi_{NN}=0 \tag{10}$$

where

$$\phi_{SS}=(1/q^2)[U^2f(f\phi_\xi)_\xi+2UVfg\phi_{\xi\eta}+V^2g(g\phi_\eta)_\eta]$$

$$\phi_{NN}=(1/q^2)[V^2f(f\phi_\xi)_\xi-2UVfg\phi_{\xi\eta}+U^2g(g\phi_\eta)_\eta] \tag{11}$$

Notice that substitution of Eqs. (11) into (10) yields the governing equation [Eq. (8)]. Thus, as pointed out by South,[10] Eq. (10) is simply a rearrangement of terms which exhibits the basic features of a local rotation to the streamline direction.

The basic concept[10,11] of the rotated scheme is to use, at supersonic points, first-order, upwind differencing in both the ξ and η directions for all contributions to ϕ_{SS}, and central differencing for all contributions to ϕ_{NN}. In this manner, the correct zone of dependence at supersonic points is built into the finite-difference scheme. At subsonic points, the normal procedure of using central differences for all derivatives directly in Eq. (8) is used. Consequently, the scheme is second-order accurate at subsonic points and first-order accurate at supersonic points. The resulting finite-difference equations are solved iteratively by using column relaxation sweeping from the upstream to downstream. In such a procedure, the values obtained during an iterative sweep can be thought of as new values, ϕ_{ij}^{+}; whereas those obtained during the previous sweep can be considered old values ϕ_{ij}. In this manner, the change from one iteration to the next can be viewed as that occurring during some artificial time step Δt, and artificial time derivatives such as ϕ_t, $\phi_{\xi t}$, ϕ_{Nt}, ϕ_{St}, and $\phi_{\eta t}$ can be considered. Of course, as the relaxation process converges, these terms become neglible.

The present approach is somewhat different, however, from that used in Refs. 10 and 11 in that time terms in the streamwise direction are not introduced implicitly as a consequence of the manner in which the difference expressions are formulated. Instead, at supersonic points, a $(-\epsilon\Delta t f/\Delta\xi)\phi_{St}$ term is added explicitly to Eq. (10) and used to control the stability and convergence of the relaxation process via the parameter ϵ. The complete finite-difference expressions are listed in the Appendix.

Numerical Stability

Jameson[11] has shown that during the iterative process the acutal equation at supersonic points is of the form

$$\chi\phi_t + (q^2/a^2 - 1)\phi_{SS} + 2\alpha\phi_{St} - \phi_{NN} + 2\beta\phi_{Nt} = 0 \qquad (12)$$

and that for numerical stability the coefficients must be such that

$$\chi = 0 \quad \alpha^2 > \beta^2(q^2/a^2 - 1) \qquad (13)$$

For the present problem, examination of the finite-difference equations shows that Eq. (13) is equivalent to[12]

$$\epsilon^2 > (V^2/q^2)(q^2/a^2 - 1) \qquad (14)$$

Notice that this requirement means that for a fixed value for ϵ, numerical instability is most likely to occur where the local Mach number is large, say immediately upstream of a shock wave. Numerical experiments have been conducted to verify Eq. (14), and in most cases instability, if present, does originate from the high Mach number region in front of a shock wave. However, the minimum value of ϵ predicted by Eq. (14) is usually much smaller than the value actually required in practice, which usually is only slightly less than ϵ_{max}, where

$$\epsilon^2_{max} \sim M^2_{max} - 1 \qquad (15)$$

Surface Boundary Conditions and Computation of Shape

As mentioned in the Introduction, in the design mode, the shape of the nose region (typically 6-10% of the chord) is specified, and the pressure is prescribed over the remainder of the airfoil. This procedure is used for several reasons. First, the nose region must be known very accurately in order to fabricate an airfoil correctly. Thus, by prescribing the nose shape, a possible major source of error is eliminated from the design procedure. Second, the boundary condition in the inverse region specifies the derivative of the perturbation potential in essentially the x direction, and a starting value must be known. With the present scheme, this value is determined by the direct solution in the nose region and need not be estimated or iterated for. Third, in some cases the designer may wish only to modify the aft portion of the airfoil. This can be done with the present scheme, since the switch point from direct to inverse can be set by an input variable anywhere from about 6% chord to the trailing edge. Finally, and perhaps most importantly, specification of the nose shape gives the designer a physical entity whereby he can control the degree of closure of the trailing edge. This feature will be discussed later.

With this philosophy, the appropriate airfoil boundary condition in the direct region near the leading edge is the surface tangency requirement

$$\left(\frac{dy}{dx}\right)_b = \frac{V_b}{U_b} = \frac{\sin\alpha + g_b\phi_{\eta b}}{\cos\alpha + f_b\phi_{\xi_b}} \qquad (16)$$

and in the inverse region, where the pressure is specified, it is

$$\phi_{x_b} = f_b\phi_{\xi_b} = -\cos\alpha + \left\{\frac{1}{1 + V_b{}^2/U_b{}^2}\left[1 - \frac{2}{(\gamma-1)M_\infty{}^2} \cdot \left(\left[1 + \frac{\gamma M_\infty{}^2 C_{pb}}{2}\right]^{(\gamma-1)/\gamma} - 1\right)\right]\right\}^{1/2} \qquad (17)$$

In order to generate dummy values of ϕ at mesh points inside the boundary such that the usual difference equations can be solved at all points outside the boundary, without creating instability, a Taylor series about the dummy point $(i,j-1)$ (see Fig. 2) is used to express $\phi_{\eta b}$ and ϕ_{ξ_b}. Thus

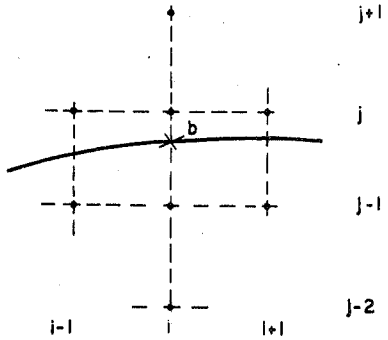

Fig. 2 Relationship between airfoil and grid (upper surface).

$$\phi_{\eta b} = \phi_{\eta i,j-1} + (\eta_b - \eta_{j-1})\phi_{\eta\eta i,j-1} + \ldots \qquad (18a)$$

$$\phi_{\xi_b} = \phi_{\xi i,j-1} + (\eta_b - \eta_{j-1})\phi_{\xi\eta i,j-1} + \ldots \qquad (18b)$$

When these are written in finite-difference form, using second-order expressions for ϕ_ξ and ϕ_η and at least first-order ones for $\phi_{\eta\eta}$ and $\phi_{\xi\eta}$, they become (for the upper surface case)

$$\phi_{\eta_b} = \frac{-3\phi_{i,j-1} + 4\phi_{ij} - \phi_{i,j+1}}{2\Delta\eta} + (\eta_b - \eta_{j-1})\left(\frac{\phi_{i,j-1} - 2\phi_{ij} + \phi_{i,j+1}}{\Delta\eta^2}\right) \qquad (19)$$

$$\phi_{\xi_b} = \frac{\phi_{i+1,j-1} - \phi_{i-1,j-1}}{2\Delta\xi} + (\eta_b - \eta_{j-1})\left(\frac{\phi_{i+1,j} - \phi_{i+1,j-1} - \phi_{i-1,j} + \phi_{i-1,j-1}}{2\Delta\xi\Delta\eta}\right) \qquad (20)$$

These expressions then can be substituted into Eq. (16) and the result solved for a sufficiently accurate $\phi_{i,j-1}$ that is in terms of the neighboring potentials, body slope, and body position.

In the inverse region, the surface pressure boundary condition must be applied at the location given for the surface by the previous relaxation sweep or last surface update. Thus, to start the inverse calculation, an initial profile is needed. Although this profile should be reasonable and compatible with the shape selected for the nose region, it is not critical, and the final airfoil may be quite different from the initial profile.

As in the direct region, the Taylor series expression for $\phi_{\xi b}$ is used in Eq. (17), but in the inverse case, considerable care must be used in selecting the finite-difference forms for $\phi_{\xi i,j-1}$ and $\phi_{\xi\eta i,j-1}$. After considerable investigation,[13] it was determined that the best form to use for $\phi_{\xi b}$ in Eq. (17) is (for the upper surface)

$$\phi_{\xi_b} = \frac{3\phi_{i,j-1} - 4\phi_{i-1,j-1} + \phi_{i-2,j-1}}{2\Delta\xi} + (\eta_b - \eta_{j-1})\left(\frac{\phi_{i+1,j} - \phi_{i+1,j-1} - \phi_{i-1,j} + \phi_{i-1,j-1}}{2\Delta\xi\Delta\eta}\right) \qquad (21)$$

This form does not introduce any numerical instabilities, builds into $\phi_{i,j-1}$ the upstream history of the airfoil, and uses C_{pbi}. It leads to smooth boundary values and airfoil shapes, with no apparent oscillations.

When Eq. (21) is substituted into Eq. (17), and the result is solved for $\phi_{i,j-1}$, the final expression involves the square of the airfoil slope $V_b{}^2/U_b{}^2$. Technically, this makes the

equation nonlinear. However, since the surface slope is usually small in the inverse region, it has been found to be sufficiently accurate to hold $(V/U)_b$ constant at the value obtained for the last airfoil surface update. For those situations in which the flow at point (i,j) is supersonic, the rotated finite-difference scheme may require a $\phi_{i,j-2}$ value as well as $\phi_{i,j-1}$. Thus, in all cases, a value of $\phi_{i,j-2}$ is determined by extrapolation as

$$\phi_{i,j-2} = -\phi_{ij} + 2\phi_{i,j-1} \tag{22}$$

The preceding procedures for determining the values of the dummy mesh points inside the boundary is performed twice for the relaxation procedure of column i. First, Eq. (16) or (17), etc., is used with ϕ values obtained by the previous relaxation sweep in order to obtain old values for the dummy points $\phi_{i,j-1}$ and $\phi_{i,j-2}$. Then, after the column i has been relaxed, they are used again with as many current values of ϕ as possible to obtain new values $\phi^+_{i,j-1}$ and $\phi^+_{i,j-2}$. In this manner, the dummy mesh points will have both old and new values, just like regular mesh points, and they can be used directly in the finite-difference formulas without special treatment. A similar procedure is used to satisfy the boundary conditions on the lower surface of the airfoil.

In the inverse case, the airfoil also must be computed by solving Eq. (16) for the surface ordinates y, as a function of x, with the initial conditions given by the slope and surface ordinate at the interface between direct and inverse regions. In the present problem, the latter, as well as starting values for Eq. (17), are known because the nose region is solved directly. If the problem were treated completely inversely, the shape would depend upon an arbitrary value for ϕ_{noise} whose value is not obvious physically.

Probably the most appealing method for solving Eq. (16) is to use Runge-Kutta of order two, either directly or with iteration, since it only requires information at i and $i+1$. This approach was tried, but it was found to be insufficiently accurate. Consequently, the Runge-Kutta method of order four has been used, and although it requires for each step information at i, $i+\frac{1}{2}$, and $i+1$, the improvement in accuracy is worth the added complexity.

In the process of solving Eq. (16), $\phi_{\eta b}$ and $\phi_{\xi b}$ must be evaluated by finite differences. Although Eq. (19) is the obvious choice for $\phi_{\eta b}$, either Eq. (20) or (21) could be used for $\phi_{\xi b}$. Both have been used and both work well, but experience indicates that more accurate airfoil shape results are obtained by use of the central-difference scheme, Eq. (20).

Finally, notice that in integrating Eq. (16) the most difficult region from an accuracy standpoint is near the leading edge, where the surface slopes are very large. In the present approach this difficulty is essentially eliminated since the nose shape is prescribed and the nose region is solved directly.

Computational Procedure

In order to start the inverse problem, an initial airfoil shape must be assumed, but this choice is not critical, and the final airfoil shape may be considerably different. Next, since experience has indicated that the inverse scheme works best if the perturbation potentials have reasonable values, 50 relaxation cycles are performed in the direct mode for the initial airfoil shape on a very coarse grid. Then, the grid spacing is halved and the inverse procedure is initiated using the input pressure distribution as the boundary condition in the inverse region.

Now an important consideration in the inverse calculations is the frequency of computing or updating the new airfoil shape. Since in the early relaxation cycles the pressure boundary condition may cause very large perturbations from the initial values, it has been found best not to start the update procedure until after the first 50 iterative cycles on the second grid, which all are in the inverse mode. After that, updating can occur after each relaxation sweep, if desired, or at some specified interval, or not until after complete convergence has been achieved. The latter is essentially the procedure used by Tranen.[7] However, since each update requires a reasonable amount of computer time, it would be inefficient to calculate a new airfoil shape after each relaxation cycle. On the other hand, not updating until after convergence has been achieved usually yields airfoil shapes not completely compatible with the desired pressure distribution. Based upon a series of tests, it appears that the optimum procedure is to perform the update airfoil shape calculation after every ten relaxation cycles. More frequent updating does not improve the accuracy of the final shape and only wastes computer time, whereas less frequent use sometimes leads to small errors in the final shape. After convergence on the second grid, the spacing is halved at least once more, and the entire procedure is repeated.

Another important consideration is the determination of convergence. In direct calculations, it usually is sufficient to monitor the maximum perturbation potential change between relaxation cycles and the number of relaxation cycles. The calculation then is stopped when either the maximum perturbation potential change is less than some specified value (i.e., 10^{-5}) or the number of cycles exceeds a given number. However, in the inverse problem, another important criterion is the maximum change that occurs between update calculations in the surface ordinates of the airfoil being designed. It has been found that this value also should be monitored, and the computations should be continued until it is consistently less than some specified value (say $\Delta y/c < 0.0001$). Frequently, this action yields a maximum perturbation potential change smaller than would be required for a direct calculation.

All of the results presented in this paper have been obtained with this procedure and have used at least two grid halvings. Usually, the final grid contained 49×49 points, with about 66 on the airfoil surfaces. Typical computation times were 5-6 min on a CDC 6600 (including Varian plots) or about 15-20 min on an IBM 360/65.

Numerical Studies

Comparisons

Any new numerical technique can be verified only by comparing its results with those previously obtained by other investigators. As suggested by Lock,[14] the NACA 0012 airfoil is an excellent test case because its shape can be exactly prescribed analytically. The solutions of Sells,[15] which are believed to have an accuracy to about 1%, can be used for comparison. Figure 3 compares analysis results obtained by the present method with those of Sells[15] for a lifting subcritical case. Here, the two sets of data are always within 2% of one another, and the lift coefficients agree exactly. In particular, notice the excellent agreement on the magnitude and location of the uppr surface pressure peak.

Figure 4 shows results for an NACA 0012 at a freestream Mach number of 0.75 and 2° angle of attack. Superimposed on this pressure distribution is a result obtained by Newman[16] using a program developed by Jameson.[17] The Jameson program, which uses conformal coordinates in the circle plane, is believed to be very accurate, and the results shown on Fig. 4 were obtained with a 192×32 grid with 192 points on the airfoil surfaces. Notice that the lift and moment coefficients essentially agree, and that the pressure coefficients and shock location agree quite well.

Similar verification of the accuracy of the present program has been obtained for biconvex and NACA 63A006 airfoils.[12] Thus, based on these comparisons, it is believed that accurate transonic flow solutions can be obtained efficiently in a Cartesian grid system, and that the present approach is valid.

Self-Consistency of Inverse Solution

When pressure results from a direct calculation are used as in input for an inverse calculation, the original airfoil shape

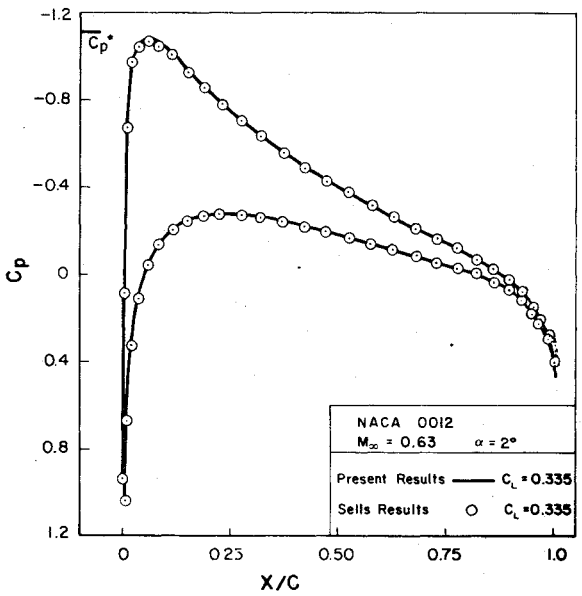

Fig. 3 Comparison with Sells for subcritical lifting case.

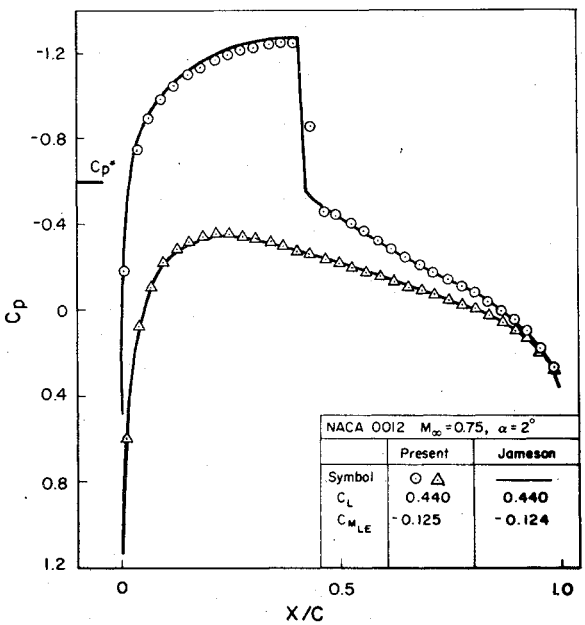

Fig. 4 Comparison with Jameson for supercritical lifting case.

should be recovered. However, as shown by Refs. 4-6, this task can be very difficult to accomplish, and the key to success is numerical consistency between the direct and inverse computations. Hence, this type of test checks not only the validity of the inverse approach, but also the consistency of the difference schemes. Several of these tests have been conducted, and some typical results for a supercritical lifting case are shown in Fig. 5. Here a strong shock, having a local upstream Mach number of about 1.30, exists on the upper surface of the NACA 0012 airfoil. Notice that the agreement between the lift coefficients and the actual and computed slopes is excellent, and that the differences between the upper and lower surface values is too small to be detected on the plot. For this case, the computed surface ordinates are everywhere within 0.33% $(T/C)_{max}$ of the actual NACA 0012 ordinates, and no problems exist near the shock or the trailing edge. Based upon these tests and results, it is believed that the present inverse design scheme and program are self-consistent and reasonably accurate.

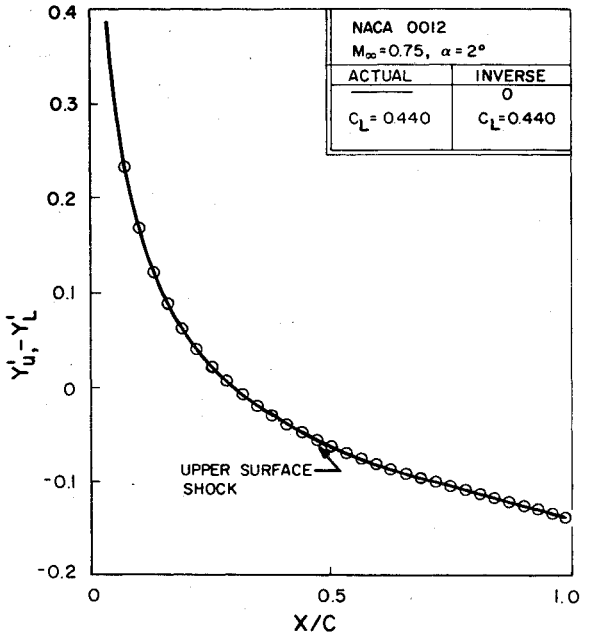

Fig. 5 Comparison of actual airfoil slopes with those computed by design program.

Application and Typical Results

When designing an airfoil to satisfy a specified pressure distribution, the final shape must have certain reasonable characteristics. For example, since the inverse approach yields the location of the boundary-layer displacement surfaces, the ordinates near the trailing edge must not criss-cross and the trailing edge should have a finite thickness. Since the displacement thickness near the trailing edge is frequently on the order of 0.4% of the chord, the computed trailing edge thickness should be on the order of 1.0% or more. Unfortunately, it is not at all obvious how the input pressure distribution should be modified to achieve such characteristics if they do not result. Besides, such a modification would change one of the desired design parameters, namely, the pressure distribution.

With the present scheme, however, the inverse pressure distribution can be kept the same, and the nose shape can be used by the designer to control the degree of tail closure. The procedure is demonstrated in Fig. 6, which shows three airfoils, each designed with the same C_p distribution from 7% chord to the trailing edge. The input pressure distribution for this case is of the shockless variety, and contains the lower surface bucket typical of aft-cambered airfoils. As can be seen on Fig. 6, airfoil no. 4 has an NACA 0012 nose shape. But, obviously, the resultant design has too thick of a trailing edge. In order to correct this deficiency, a nonsymmetrical nose shape having a smaller leading-edge radius was tried. The resultant design, termed airfoil no. 5 on Fig. 6, is about 2% thinner and has a more reasonable trailing edge shape. Finally, in order to create an even thinner airfoil and trailing edge, the lower surface nose region ordinates were raised by 0.1% of the chord; the results are shown as airfoil no. 6.

Figure 7 shows another case in which the nose shape was used to control the trailing edge characteristics. The pressure distribution for these airfoils, which is the solid curve in Fig. 8, was selected to have the same basic lift coefficient and lower surface pressure distribution as an NACA 0012 at the same flight conditions, but without the strong upper surface shock wave. In each case, the nose shapes and initial starting profiles were those associated with NACA 00XX airfoils. For the NACA 0010 nose shape, airfoil no. 100, the upper and lower surfaces of the designed airfoil criss-crossed; as can be seen on Fig. 7 for airfoils 110 and 115, as the leading edge

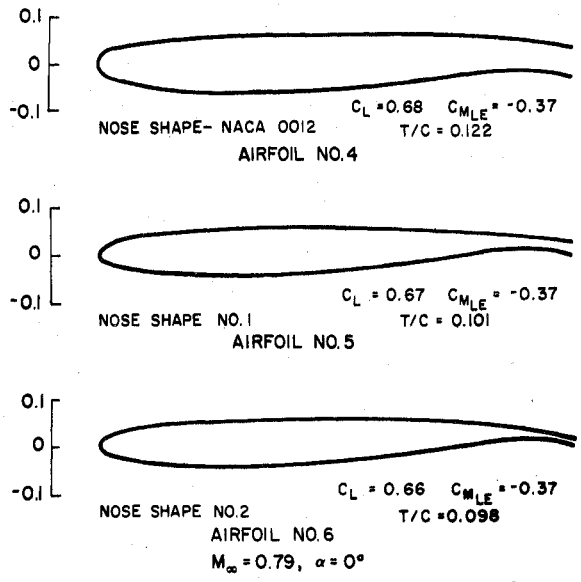

Fig. 6 The use of nose shape to control trailing edge closure, example 1.

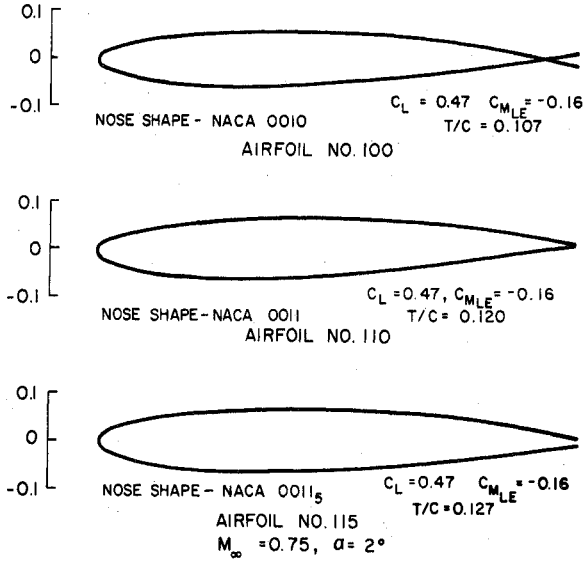

Fig. 7 The use of nose shape to control trailing edge closure, example 2.

radius was increased, the maximum and trailing edge thickness also increased proportionately.

Based upon the results shown in Figs. 6 and 7, it is believed that the nose shape can be used to control the trailing edge shape, and that any reasonable thickness of the trailing edge displacement surfaces can be achieved by the designer by adjusting the nose shape. As indicated previously, this adjustment does not require changing the desired inverse C_p distribution.

A severe test for a design program is whether or not an analysis or direct solution of the designed airfoil returns the design of inverse C_p distribution. Figure 8 compares the inverse C_p used to design airfoil no. 115 with that obtained from a direct solution (airfoil given) using the ordinates for no. 115. In this comparison, the C_p input for the inverse calculation is computed by backward differences for $\phi_{\xi b}$ [Eq. (21)], whereas the direct C_p results are based upon the more usual central differences. As a result, perfect agreement should not be expected. Nevertheless, the agreement in the C_p distribution and lift coefficients is excellent and tends to verify the validity and accuracy of the present inverse design program. Similar agreement between direct and inverse results has also been obtained for airfoil no. 5.

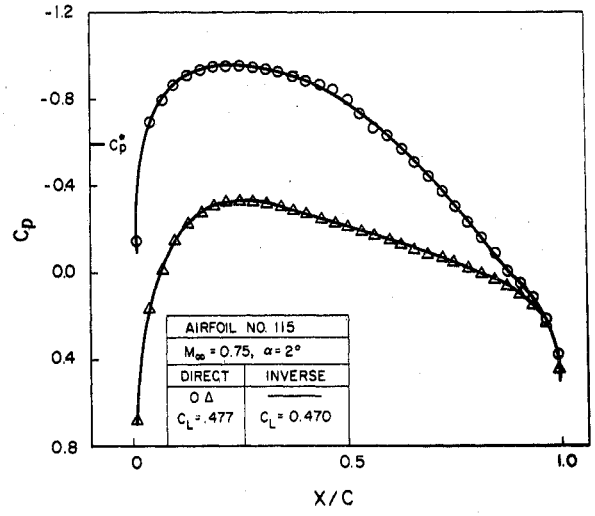

Fig. 8 Comparison of inverse C_p distribution with that obtained by analysis of designed airfoil.

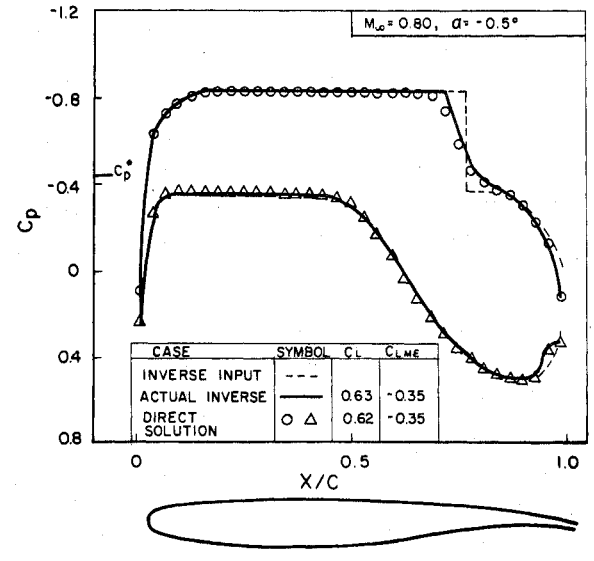

Fig. 9 Comparison of C_p distributions.

A final case is shown in Fig. 9. An arbitrary pressure distribution (dashed line) having an upper surface Mach number plateau around 1.2, followed by a large jump to subsonic flow at 76% chord, was selected for the inverse input. No attempt was made to match the discontinuity to shock jump conditions. On the lower surface, the C_p was chosen to maintain subsonic flow. However, a bucket selected according to the Stratford separation criteria[18] was included to enhance lift. As indicated, the design program uses a backward-difference scheme with the C_p input; thus, in regions of large gradients, the output, which is computed by a central scheme and should be more accurate, may be slightly different.

In the course of the inverse solution, the trailing edge displacement surfaces that satisfied the input C_p distribution were not parallel, and, thus, the inviscid solution required a rear stagnation-point behavior. The actual inverse pressure distribution, which was computed by central differences and is indicated on Fig. 9 by the solid line, shows this behavior. In addition, notice that the upper surface discontinuity has been smoothed. Examination of the flowfield results shows a smooth supersonic bubble on the upper surface and indicates that the decelleration, although rapid, is not due to a shock wave of any significant strength. Also portrayed are the results of a direct solution for the designed airfoil which exhibit excellent agreement with the actual inverse pressure

coefficient distribution. Finally, the airfoil shown is the shape obtained after an estimate for the boundary-layer displacement thickness, calculated by the method of Nash-McDonald for a Reynolds number of 20,000,000, has been subtracted.

It is believed that the results of Fig. 9 demonstrate that the present inserve technique and program can handle "arbitrary" pressure inputs. In addition, it will yield verifiable results consistent with physical reality, even if the input pressure distribution is not.

Concluding Remarks

A technique suitable for designing two-dimensional transonic airfoils having a specified pressure distribution, or for analyzying the flow about specific airfoils, has been developed. This method utilizes the full inviscid potential flow equation and exact boundary conditions and solves them via numerical relaxation. A rotated finite-difference scheme is employed in order to obtain the correct domain of dependence in supersonic regions, and Jameson's time-like damping is included to insure numerical stability. Further, grid halving is used to achieve computational efficiency.

By use of this method, which includes simultaneous airfoil update, a logical method for controlling trailing edge closure has been developed. In addition, it has been demonstrated by comparison with previous results that it is not necessary to match the computational grid to the airfoil surface and that accurate, numerically consistent, and physically correct results can be obtained in a Cartesian grid system. The technique has been used to analyze and design aft-cambered and other airfoils specifically for transonic flight.

Appendix

The finite-difference expressions used in the present formulation are: for contributions to ϕ_{NN} when $q^2 > a^2$

$$(f\phi_\xi)_\xi = (1/\Delta\xi^2)\{f_{i+1/2}(\phi_{i+1,j}-\phi_{ij}) - f_{i-1/2}(\phi^+_{ij}-\phi^+_{i-,j})\} \tag{A1}$$

$$\phi_{\xi\eta} = (1/4\Delta\xi\Delta\eta)\{\phi^+_{i-1,j} - \phi^+_{i-1,j+1} - \phi_{i+1,j-1} + \phi_{i+1,j+1}\} \tag{A2}$$

$$(g\phi_\eta)_\eta = (1/\Delta\eta^2)\{g_{j+1/2}(\phi^+_{i,j+1}-\phi^+_{ij}) - g_{j-1/2}(\phi^+_{ij}-\phi^+_{i,j-1})\} \tag{A3}$$

For contributions to ϕ_{SS} when $q^2 > a^2$ and $V > 0$

$$(f\phi_\xi)_\xi = (1/\Delta\xi^2)\{f_{i-1/2}(\phi_{ij}-\phi_{i-1,j}) - f_{i-3/2}(\phi_{i-1,j}-\phi_{i-2,j})\} \tag{A4}$$

$$\phi_{\xi\eta} = (1/\Delta\xi\Delta\eta)\{\phi_{ij} - \phi_{i-1,j} - \phi_{i,j-1} + \phi_{i-1,j-1}\} \tag{A5}$$

$$(g\phi_\eta)_\eta = (1/\Delta\eta^2)\{g_{j-1/2}(\phi_{ij}-\phi_{i,j-1}) - g_{j-3/2}(\phi_{i,j-1}-\phi_{i,j-2})\} \tag{A6}$$

where, to create stability, there is added to the basic equation

$$\frac{-\epsilon\Delta t}{\Delta\xi} f\phi_{S_t} = \frac{-\epsilon f\Delta t}{\Delta\xi}\left[\frac{Uf}{q}\phi_{\xi t} + \frac{Vg}{q}\phi_{\eta t}\right]$$

$$= \frac{-\epsilon f}{\Delta\xi}\left[\frac{Uf_{i-1/2}}{\Delta\xi q}(\phi^+_{ij}-\phi_{ij}-\phi^+_{i-1,j}+\phi_{i-1,j}) + \frac{V}{q}\frac{g_{j-1/2}}{\Delta\eta}(\phi^+_{ij}-\phi_{ij}-\phi^+_{i,j-1}+\phi_{i,j-1})\right] \tag{A7}$$

For contributions to ϕ_{SS} when $q^2 > a^2$ and $V < 0$

$$(f\phi_\xi)_\xi = (1/\Delta\xi^2)\{f_{i-1/2}(\phi_{ij}-\phi_{i-1,j}) - f_{i-3/2}(\phi_{i-1,j}-\phi_{i-2,j})\} \tag{A8}$$

$$\phi_{\xi\eta} = (1/\Delta\xi\Delta\eta)\{-\phi_{ij} + \phi_{i-1,j} + \phi_{i,j+1} - \phi_{i-1,j+1}\} \tag{A9}$$

$$(g\phi_\eta)_\eta = (1/\Delta\eta^2)\{g_{j+1/2}(\phi_{ij}-\phi_{i,j+1}) - g_{j+3/2}(\phi_{i,j+1}-\phi_{i,j+2})\} \tag{A10}$$

and to create stability there is added

$$\frac{-\epsilon f\Delta t}{\Delta\xi}\phi_{St} = \frac{-\epsilon f}{\Delta\xi}\left[\frac{U}{q}\frac{f_{i-1/2}}{\Delta\xi}(\phi^+_{ij}-\phi_{ij}-\phi^+_{i-1,j}+\phi_{i-1,j}) + \frac{V}{q}\frac{g_{j+1/2}}{\Delta\eta}(-\phi^+_{ij}+\phi_{ij}+\phi^+_{i,j+1}-\phi_{i,j+1})\right] \tag{A11}$$

At points where $q^2 < a^2$, the expressions are

$$(f\phi_\xi)_\xi = (1/\Delta\xi^2)\{f_{i+1/2}\phi_{i+1,j} - (f_{i+1/2}+f_{i-1/2})[(\phi^+_{ij}/w) + (1-1/w)\phi_{ij}] + f_{i-1/2}\phi^+_{i-1,j}\} \tag{A12}$$

$$\phi_{\xi\eta} = (1/4\Delta\xi\Delta\eta)\{\phi^+_{i-1,j-1} - \phi^+_{i-1,j+1} - \phi_{i+1,j-1} - \phi_{i+1,j+1}\} \tag{A13}$$

$$(g\phi_\eta)_\eta = (1/\Delta\eta^2)\{g_{j+1/2}(\phi^+_{i,j+1}-\phi^+_{ij}) - g_{j-1/2}(\phi^+_{ij}-\phi^+_{i,j-1})\} \tag{A14}$$

where the relaxation factor w has been incorporated into the difference formulas. In all cases, the velocities U and V are represented by central differences, using old values. When these expressions are substituted appropriately into Eqs. (10) and (11) or Eq. (8), the result is a triagonal system of equations that can be solved for the values of ϕ^+_{ij} on column i.

References

[1] Nieuwland, G. Y., "Transonic Potential Flow Around a Family of Quasi-Elliptical Aerofoil Sections," National Lucht-en Ruimtevaart Laboratorium, Amsterdam, NLR-TR-T. 172, 1967.

[2] Bauer, F., Garabedian, P., and Korn, D., *A Theory of Supercritical Wing Sections, with Computer Programs and Examples*, Springer-Verlag, 1972.

[3] Hicks, R. M., Murman, E. M., and Vanderplaats, G. N., "An Assessment of Airfoil Design by Numerical Optimization," NASA TM X-3092, July 1974.

[4] Erdos, J., Baronti, P., and Elzweig, S., "Transonic Viscous Flow Around Lifting Two-Dimensional Airfoils," AIAA Paper 72-678, Boston, Mass., June 1972.

[5] Steger, J. L. and Klineberg, J. M., "A Finite-Difference Method for Transonic Airfoil Design," *AIAA Journal*, Vol. 11, May 1973, pp. 628-635.

[6] Carlson, L. A., "Inverse Transonic Flow Calculations Using Experimental Pressure Distributions," *AIAA Journal*, Vol. 12, April 1974, pp. 571-572.

[7] Tranen, T. L., "A Rapid Computer Aided Transonic Airfoil Design Method," AIAA Paper 74-501, Palo Alto, Calif., June 1974.

[8] Whitcomb, R. T., "Review of NASA Supercritical Airfoils," *Proceedings of the IXth ICAS Congress*, Haifa, Israel, Paper 74-10, Aug. 1974.

[9] Ludford, G. S. S., "The Behavior at Infinity of the Potential Function of a Two Dimensional Subsonic Compressible Flow," *Journal of Mathematical Physics*, Vol. 30, Oct. 1951, pp. 117-130.

[10] South, J. C., Jr. and Jameson, A., "Relaxation Solutions for Inviscid Axisymmetric Transonic Flow Over Blunt or Pointed Bodies," *Proceedings AIAA Computational Fluid Dynamics Conference*, Palm Springs, Calif., July 1973, pp. 8-17.

[11] Jameson, A., "Iterative Solution of Transonic Flows Over Airfoils and Wings, Including Flows at Mach 1," *Communications on Pure and Applied Mathematics*, Vol. 27, 1974, pp. 283-309.

[12] Carlson, L. A., "Transonic Airfoil Flowfield Analysis Using Cartesian Coordinates," NASA CR-2577, 1975.

[13] Carlson, L. A., "Transonic Airfoil Design Using Cartesian Coordinates," NASA-CR-2578, 1976.

[14] Lock, R. C., "Test Cases for Numerical Methods in Two-Dimensional Transonic Flows," AGARD Rept. R-575-70, 1970.

[15] Sells, C. C. L., "Plane Subcritical Flow Past a Lifting Airfoil," Royal Aircraft Establishment, Farnborough, England, 67146, 1967.

[16] Newman, P. A., *Theoretical Aerodynamics Branch*, NASA Langley, private communication, 1974.

[17] Jameson, A., "Transonic Flow Calculations for Airfoils and Bodies of Revolution," Grumman Aerodynamics Rept. 390-71-1, Dec. 1971.

[18] Stratford, B. S., "The Prediction of Separation of the Turbulent Boundary Layer," *Journal of Fluid Mechanics*, Vol. 5, 1959, pp. 1-16.